

# A Wirelessly Powered, Biologically Inspired Ambulatory Microrobot

Michael Karpelson, Benjamin H. Waters, Benjamin Goldberg, Brody Mahoney,  
 Onur Ozcan, Andrew Baisch, Pierre-Marie Meyitang, Joshua R. Smith, and Robert J. Wood

**Abstract**—Onboard power remains a major challenge for miniature robotic platforms. Locomotion at small scales demands high power densities from all system components, while limited payload capacities place severe restrictions on the size of the energy source, resulting in integration challenges and short operating times when using conventional batteries. Wireless power delivery has the potential to allow microrobotic platforms to operate autonomously for extended periods when near a transmitter. This paper describes the first demonstration of RF wireless power transfer in an insect-scale ambulatory robot. A wireless power transmission system based on magnetically coupled resonance is designed for the latest iteration of the Harvard Ambulatory MicroRobot (HAMR), a piezoelectrically driven quadruped that had previously received power through a tether. Custom power and control electronics are designed and implemented on lightweight printed circuit boards that form a part of the mechanical structure of the robot. The integration of the onboard receiver, power and control electronics, and mechanical structure yields a 4cm, 2.1g robot that can operate autonomously in two wireless power transmission scenarios.

## I. INTRODUCTION

Miniature robots inspired by ambulatory insects offer great potential in such applications as search-and-rescue, hazardous environmental exploration, and infrastructure inspection. Swarms of inexpensive, mass-produced robotic insects with locomotion capabilities similar to their biological counterparts could traverse terrain and penetrate spaces inaccessible to humans and large-scale robots, executing complex, challenging missions through collective behaviors and a high degree of redundancy. However, implementing self-contained energy sources is extremely challenging in insect-scale robots due to the lack of appropriately sized batteries with high power and energy densities [1] and the increase in cost of transport at lower scales [2], while any form of tethered power delivery can severely restrict the mobility and reliability of microrobotic platforms.

Wireless power is a viable option to replace or complement state-of-the-art battery technology in any application where robots can remain in close proximity to a transmitter when operating or recharging an onboard battery. In one scenario, robots could receive power through walls, floors, or ceilings, allowing them to perform inspection and repair tasks inside the walls or between the floors of a building (Fig. 1(a)).

M. Karpelson, B. Goldberg, O. Ozcan, A. Baisch, P.-M. Meyitang, and R. J. Wood are with the School of Engineering and Applied Sciences and the Wyss Institute for Biologically Inspired Engineering, Harvard University, Cambridge, MA 02138 (contact e-mail: michael.karpelson@wyss.harvard.edu)

B. H. Waters, B. Mahoney, and J. R. Smith are with the Department of Computer Science and Engineering, University of Washington, Seattle, WA 98195 (contact e-mail: bhw2114@uw.edu)

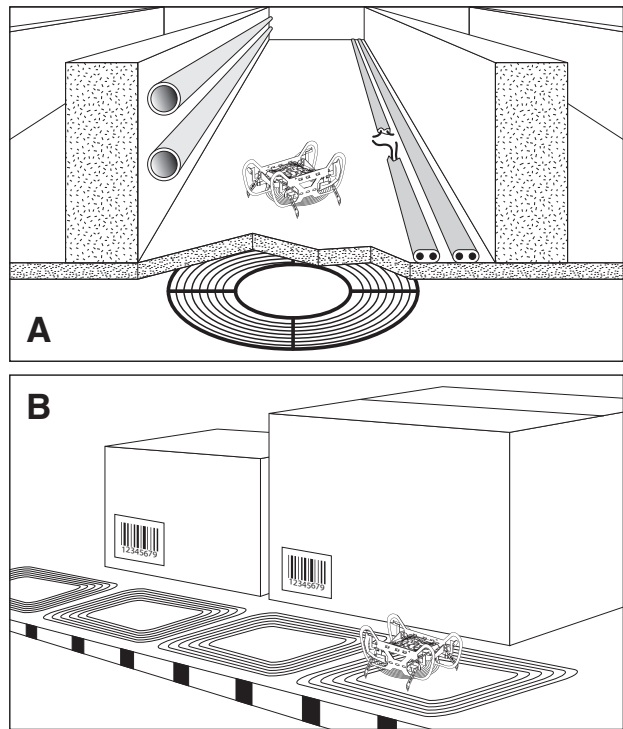


Fig. 1. Conceptual scenarios of wireless power delivery to microrobots: inspection and repair tasks inside the walls or between the floors of a building (a), and operation in a structured environment with multiple embedded transmitters, such as a factory or warehouse (b).

Wireless power can also prove advantageous in structured environments with multiple transmitters embedded throughout an area, such as a factory floor, warehouse, or building conduit (Fig. 1(b)).

The Harvard Ambulatory MicroRobot (HAMR) is a biologically inspired, insect-scale robotic platform, currently in its fifth mechanical design iteration. Previous versions of HAMR have demonstrated short-term autonomous operation using battery power [3], controlled high-speed locomotion with external power [4], and the application of novel fabrication techniques suitable for mass production [5]. Onboard power for HAMR is complicated not only by the small scale and limited payload capacity of the robot, but also by the operational requirements of the high energy density piezoelectric actuators [6] used to drive its legs. These actuators require high-voltage, time-varying drive signals in the range of 200-300V and 1-50Hz, introducing significant challenges in the design of power and drive electronics, and translating to overall input power requirements on the order of 10mW to 1W, depending on gait frequency. Wireless

power transmission can provide onboard voltages in the tens of volts; while not enough to drive piezoelectric actuators directly, this allows for more compact and efficient voltage conversion circuits.

Previously, resonant-based wireless power techniques have been used to demonstrate wireless operation of simple centimeter-scale wheeled robots on a surface surrounded by a transmit coil [7], while inductive techniques have seen application in robotic micromanipulation and microassembly [8]. Biomedical applications, such as capsule endoscopy, have also been investigated [9]. This work leverages the HAMR platform to demonstrate the first application of RF wireless power transmission to an insect-scale ambulatory robot. Section II reviews the principles of wireless power transmission based on magnetically coupled resonance (MCR) and describes the design and characterization of a wireless power system suitable for HAMR. Section III discusses the design and fabrication of HAMR's mechanical and electronic components, including the wireless power receiver, voltage conversion circuits, high-voltage drive circuits, and control logic. Finally, Section IV presents initial experimental results from a fully integrated, wirelessly powered HAMR, including open-loop autonomous locomotion.

## II. WIRELESS POWER TRANSMISSION

Implementing wireless power in an insect-scale robot presents a number of challenges. HAMR's 0.01-1W input power requirements and 1.5g maximum payload capacity make far-field wireless power transfer, such as radiated electromagnetic energy, difficult to implement. The efficiency of far-field wireless power techniques is typically less than 1%, which would require a very large power amplifier on the transmit side to accommodate the maximum load of HAMR [10]. There have recently been demonstrations of microwave wireless power transfer using phased-array antennas and beam-forming techniques to deliver 1W over a range of 10m [11]. However, this technique also requires a very large transmit antenna array and suffers from poor efficiency.

Near-field techniques, such as inductive coupling and MCR, provide far better efficiency at the expense of range. The range of an efficient MCR system is proportional to the size of the transmit and receive coils. Implementing wireless power transfer using MCR on a microrobot requires the receive coil to be minimized for weight, but large enough for efficient power transfer at the desired operating range. Therefore, the design of the transmit and receive coils has a significant impact on the capabilities of a wireless power system for microrobotic applications.

Two different wireless power transfer configurations have been implemented. Both scenarios can be envisioned from Fig. 2. First, a single transmit loop and coil deliver power to a receive coil mounted on HAMR such that the system achieves highest peak efficiency for the greatest axial separation distance ( $d$ ) between the transmit and receive coils. This first scenario could be used to deliver power efficiently through a thick wall or table to a microrobot, as in Fig. 1(a).

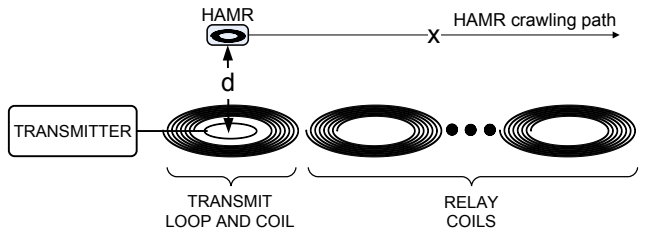


Fig. 2. Block diagram of the wireless power configurations.

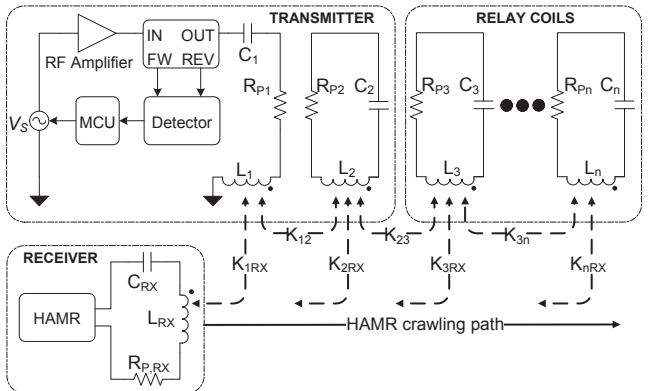


Fig. 3. Equivalent circuit diagram of the wireless power configurations.

Second, one transmit loop and coil along with several passive relay coils can be used to maintain constant power delivery to HAMR as it crawls along the coil array. The goal of this scenario is to achieve high average efficiency over the longest horizontal distance ( $x$ ) between the transmit coil and receiver. This second scenario provides power across an entire floor (or wall), such that the microrobot can crawl freely along the entire surface area of the coils, as in Fig. 1(b). The relay coils can also be placed in a two-dimensional grid spanning an entire floor or wall.

### A. Design of the Wireless Power Transfer System using Magnetically Coupled Resonators

The most basic coil topology is a 2-element system, which comprises one transmit coil and one receive coil. Although this simple configuration reduces the size and weight of both the transmit and receive coils, the range at which efficient power transfer occurs is less than that of a 3 or 4-element system [12]. A 4-element system can substantially increase the range of wireless power transfer. However, the transmit and receive resonators both require a coil and an additional loop. The added weight from the receive loop diminishes the potential improvement in range because the receive coil must shrink in size to maintain the same overall weight. Also, miniaturizing a properly tuned 4-element system is problematic due to the precision necessary for optimal loop-to-coil coupling [13]. A 3-element system consisting of a transmit loop and coil, and a receive coil, presents a compromise between the 2 and 4-element systems – it extends the range of the 2-element system while minimizing the weight and complexity of the receive coil configuration. Therefore, a

TABLE I

EXPERIMENTAL COIL GEOMETRIES AND PARASITIC COIL PARAMETERS

PARAMETER	BLUE TX COIL	GOLD TX COILS	RX COIL
L ( $\mu\text{H}$ )	3.78	2.84	3.25
C ( $\text{pF}$ )	36	4.9	42
R ( $\Omega$ )	0.9394	8.83	2.71
Q	331.6	272.9	102.6
F (MHz)	13.56	13.48	13.56
# Turns	6	9	6
OD (mm)	14.2	25.6*, 17.0**	30.0
ID (mm)	5.4	19.0*, 10.0**	27.8
AWG	14 (1.63mm)	18 (1.024mm)	33 (0.18mm)
Weight (mg)	n/a	n/a	180.0

\* Width of major axis for rounded rectangular coil

\*\* Width of minor axis for rounded rectangular coil

3-element system has been selected for this application, with the option of including any number of additional relay coils.

Fig. 3 shows the equivalent circuit schematic for the 3-element wireless power system. The transmitter consists of a signal generator that passes a radio-frequency (RF) signal to an AR Modular KAA2030 Class A power amplifier (PA). The output of the PA passes through a bi-directional coupler to inductor  $L_1$ , a single-turn loop with parasitic resistance  $R_{P1}$ , and tuning capacitor  $C_1$ . The attenuated forward and reflected waves from the directional coupler are passed to an RF magnitude and phase detector. These values can be sampled at up to 200kHz by the microcontroller unit (MCU). This feedback loop can be used for frequency tracking by minimizing the amount of reflected RF energy and for providing some indication of the power delivered to the load without requiring an additional radio communication link, which would add cost and weight to the receiver [14]. The transmit loop couples to the transmit coil  $L_2$  with coupling coefficient  $k_{12}$ . Passive relay coils can extend the range of wireless power transfer. Without the relay coils, the transmitter and receiver form a 3-element wireless power system. With the relay coils, the receive coil will receive power from the nearest relay coil.

The size and quality factor (Q) of the receive coil should be maximized for long range and highly efficient wireless power transfer. A larger receive coil means more magnetic flux can be captured from a transmit coil at greater separation distances, and higher Q implies higher efficiency. High Q requires high inductance and low resistance: the coil needs to have enough turns to maximize the inductance while using a wire gauge (AWG) that is thick enough to minimize resistance and loss. However, the weight and the outer diameter (OD) of the receive coil are limited in this application by the maximum payload capacity and the physical size of the microrobot. Therefore the receive coil design requires careful optimization of the number of turns, conductor diameter, and coil diameter for the highest Q constrained by the maximum allowable weight (180mg) and maximum outer

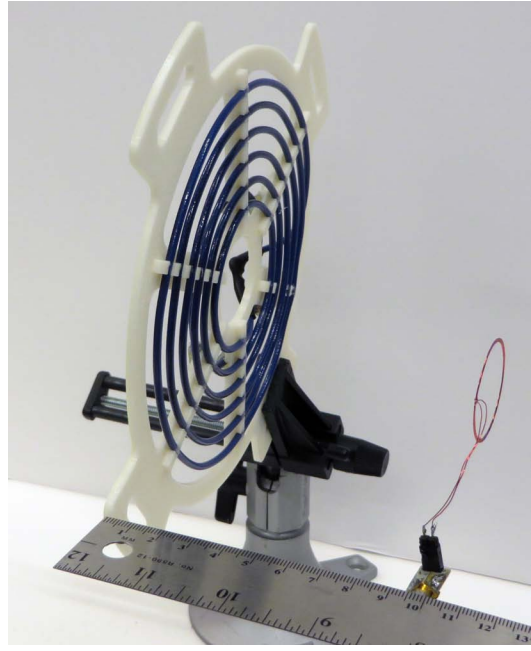


Fig. 4. The blue transmit coil and receive coil used to demonstrate high peak efficiency.

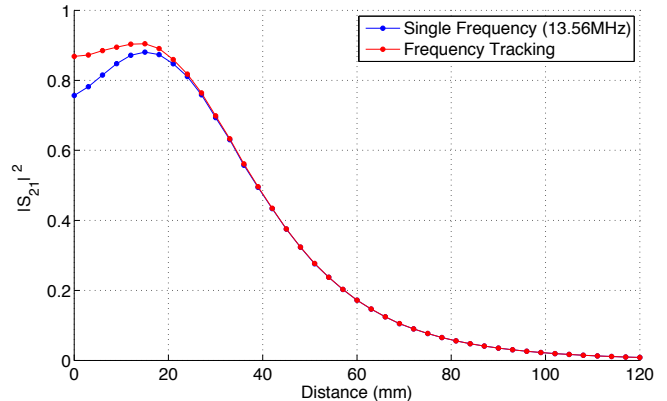


Fig. 5. Plot of  $|S_{21}|^2$  for the blue transmit coil.

diameter (30mm) to physically fit on HAMR. The receive coil is visible in Figures 4 and 6. Its electrical and geometric parameters are summarized in Table I along with all of the transmit coil parameters.

#### B. High Peak Efficiency Wireless Power System

The first transmit coil configuration, shown in Fig. 4, consists of a single-turn drive loop and multi-turn coil. The size and geometry of the blue transmit coil have been optimized, given the 30mm outer diameter of the receive coil, to maximize efficiency over the longest axial separation distance.

An HP8753ES vector network analyzer (VNA) is used to extract scattering parameters (S-parameters) for a range of distances between the coil and  $|S_{21}|^2$  has been plotted in Fig. 5.  $|S_{21}|^2$  is indicative of efficiency, and  $|S_{21}|^2 > 90\%$  can be achieved up to 20mm away from the transmitter, which would efficiently power the microrobot through a

thin wall or table. The maximum range is determined by the maximum output power of the PA (100W). HAMR can receive sufficient power, even under the maximum load condition of 1W, up to distances beyond 117mm where efficiency drops below 1%. If the outer diameter of the transmit coil decreases, the efficiency drop will occur at a shorter separation distance and will also decline more rapidly. If the transmit coil size increases, the efficiency peak will decrease because there will be less magnetic coupling between the two coils.

### C. High Average Efficiency Wireless Power System

The second coil configuration uses relay coils to extend the range of the wireless power transfer across a larger surface area. This topology is shown in Fig. 6(a-d) for one transmit coil and three, two, one, and zero relay coils, respectively. The design goal for these coils is to achieve a maximally flat magnetic field distribution across the surface of the transmit and relay coils so HAMR can crawl along the surface of any coil and achieve relatively constant efficiency. Therefore, the turn-to-turn pitch gradually increases towards the center of the coil, and ideally the turns should extend all the way to the center of the coil for maximally flat designs [15]. However this is not possible for the selected coil geometry because the coil is already self-resonant at 13.56MHz with 9 turns and cannot be tuned for 13.56MHz if the inductance increases further. The rounded rectangular coil shape is selected so that the coils can be placed in a horizontal grid with a minimally disruptive transition when crawling from one coil to the next. The coils are mounted beneath a 1/8" acrylic sheet that measures 25.6x19cm according to the largest dimensions of each coil.

The most challenging aspect of the design is sizing the transmit loop, which is only present on the transmit coil. The size of the loop is proportional to the loop-coil coupling coefficient  $k_{12}$ . If  $k_{12}$  is high, then high efficiency can only be achieved if HAMR is above the transmit coil, but efficiency drops off significantly if it is above any of the relay coils. Similarly, if  $k_{12}$  is low (i.e. small loop size), then high efficiency is achieved above the relay coils, but not the transmit coil. The loop size is optimized for equivalent efficiency above both the transmit coil and the relay coils.

A linear actuator, visible in Fig. 6(a), is used to move the receive coil along the coil array. Four separate sets of S-parameter measurements are extracted using the VNA for each of the coil configurations shown in Fig. 6. In each case, the zero distance point is set at the left side of the transmit coil and the distance is incremented in 5mm steps up to the rightmost edge of the last coil in the given configuration. The results for  $|S_{21}|^2$  are shown in Fig. 7.

For each additional relay coil, the peak and average  $|S_{21}|^2$  both drop because of the increased loss from parasitic resistances and coupling coefficients. The average  $|S_{21}|^2$  for the configuration with the transmit coil only is 0.323 with a standard deviation of 0.066. The transmit coil and one relay coil achieve an average efficiency of 0.254 and standard deviation of 0.079. Two relay coils show an average of 0.221

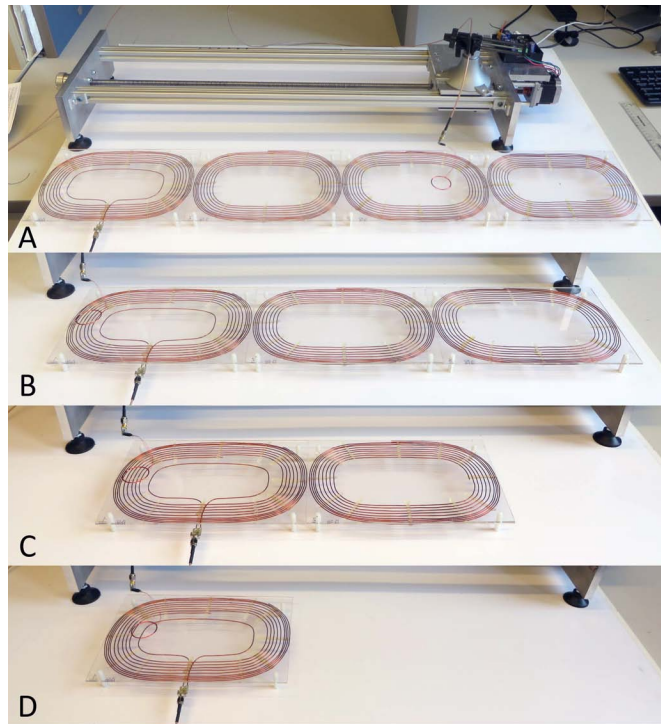


Fig. 6. Picture of the gold coils used for maintaining a constant average efficiency.

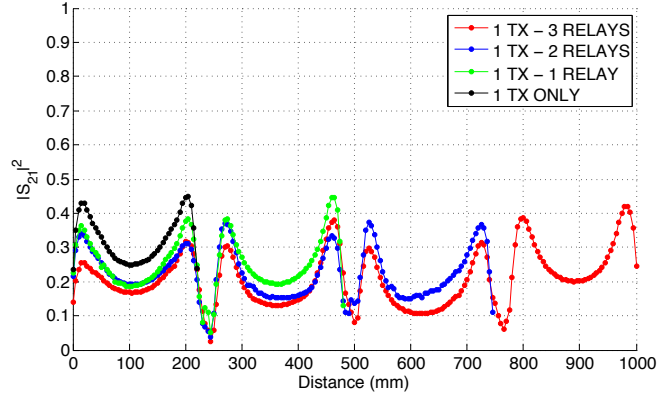


Fig. 7. Plot of  $|S_{21}|^2$  for the gold coils using frequency tracking.

with a standard deviation of 0.073, and, finally, three relay coils achieve an average of 0.208 with a standard deviation of 0.081. This final result confirms that a 30mm receive coil can be powered at a distance of 1m away from the transmit coil (nearly 330 times larger than the receive coil diameter) with an average efficiency of 0.208.

Between two adjacent coils, there is always a dip in  $|S_{21}|^2$  because the magnetic fields between the respective relay coil and the receive coil destructively interfere. However,  $|S_{21}|^2$  always remains above the minimum required efficiency (1%) for power delivery to HAMR. Lastly, as more relay coils are added to the system, additional resonant modes are excited [16]. This phenomenon emphasizes the need for frequency tracking because the optimal frequency for efficient wireless power transfer will change depending on the number of modes.

### III. MICROROBOT DESIGN AND FABRICATION

#### A. Mechanical Design and Manufacturing

The robot used in this work is mechanically identical to HAMR-VP, the first robot designed and built using the “pop-up book MEMS” manufacturing paradigm that is capable of locomotion [5]. It is designed to be a quadruped instead of a hexapod in order to decrease the fabrication complexity, and it maintains stability due to its sprawled stance. Each HAMR-VP leg has two degrees of freedom (DOF) and can move up and down (lift) as well as forward and backward (swing). Forward locomotion is achieved by actuating the two DOFs with a  $90^\circ$  phase difference, which causes a box-like motion of the feet.

The lift and swing DOFs are actuated using optimal energy density piezoelectric bimorph cantilevers [6], selected due to their simple geometry, scalability, compatibility with pop-up book MEMS, and successful implementations in other miniature robots [17], [18]. Each actuator comprises a carbon fiber core sandwiched between two  $127\mu\text{m}$  thick lead-zirconate-titanate (PZT-5H) plates, as well as a patterned copper-clad FR-4 layer for electrical and mechanical connections. The swing DOFs of the front and rear leg pairs are coupled such that when one leg swings forward, the other swings back. This simplifies the transmission and reduces the number of actuators from eight to six. Four-bar slider-crank transmissions amplify actuator outputs and transfer them to a spherical five-bar (SFB) hip joint, which couples the lift and swing DOFs and transfers motion to the leg. The SFB design was introduced in HAMR2 [19] and also implemented in HAMR3 [3], HAMR-V [4], and HAMR-VP [5]. A detailed description of the mechanical design of HAMR-VP can be found in [5].

The body, actuators, printed circuit boards (PCBs), and legs of HAMR-VP are manufactured separately to allow modularity; differently sized actuators, boards, and legs are frequently used to create alternate HAMR versions for different applications. The fabrication process for all of HAMR’s components is based on laser micromachining and lamination of different material layers (e.g. PZT for actuators, FR4 for PCBs). For example, HAMR’s body consists of 23 individual material layers that are patterned using a diode-pumped solid-state (DPSS) laser and bonded together to form four sub-laminates, each comprising five layers: carbon fiber, acrylic adhesive, Kapton, acrylic adhesive, carbon fiber. The sub-laminates, which incorporate rigid links and flexible joints, are selectively bonded together by 3 additional layers of adhesive and unfold to form the body. Fig. 8 shows the sub-laminates and the unfolding process. Additional details on fabrication can be found in [5] and [18].

#### B. Electronic Design

Fig. 9 shows a schematic of the onboard electronics package designed for the wirelessly powered HAMR. Power is delivered via the receive coil, tuning capacitor  $C_{TUNE}$ , and the rectifier, as described in Section II. Since the rectified voltage may vary depending on the distance from and orientation with respect to the transmit coil, the power conversion

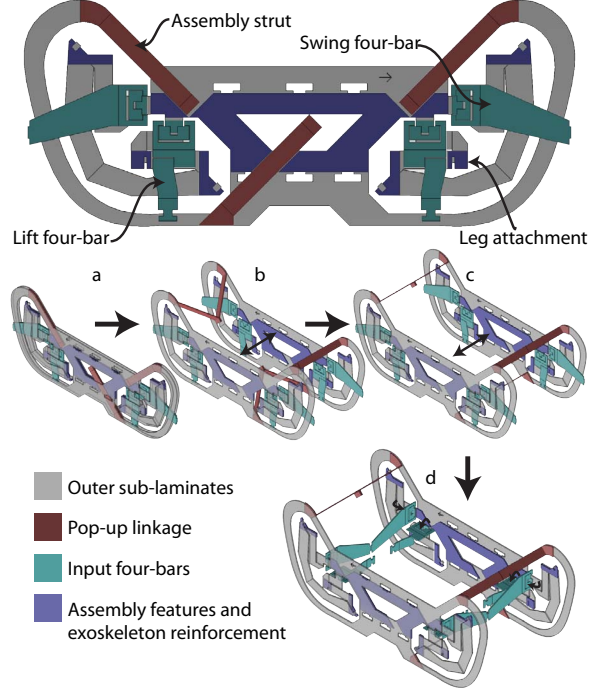


Fig. 8. The outer sub-laminates (gray) form the exoskeleton and the four SFBs. The inner sub-laminates contain the pop-up linkages, assembly features, and input four-bars. (a) HAMR body after lamination. (b) Separation of inner sub-laminates. (c) Extension to final width, constrained by pop-up linkages. (d) Deployment of four-bars by manual folding.

circuits are designed to operate with an input voltage ranging from 10V to 35V. HAMR converts the input voltage to a high-voltage supply used to drive the piezoelectric actuators, which can be configured to deliver up to 300V, and to a low-voltage supply for the control logic, configured at 4.5V. Since the high-voltage supply accounts for the majority of power consumption, a tapped inductor switching boost converter is used to maximize efficiency; the control logic consumes relatively little power, and therefore an adjustable linear regulator (LM317L-N) is used to generate the low-voltage supply to minimize mass and footprint.

The tapped inductor boost converter operates by modulating switch  $Q_B$  to periodically store energy in the primary winding  $L_P$  of the tapped inductor and deliver it to output capacitor  $C_{HV}$  via the primary and secondary windings and the diode  $D_{HV}$ . The output voltage is monitored by the onboard Atmel ATmega168PA 8-bit microcontroller via a resistive divider, and a conventional pulse frequency modulation scheme produces a constant high voltage across  $C_{HV}$  for a range of load currents. Additional details on this topology can be found in [20] and [21].

The high voltage is converted into a time-varying drive signal for the piezoelectric bimorph actuators (represented by capacitances  $C_{A1}$  and  $C_{A2}$ ) by an array of high-voltage drive circuits, one per actuator. These are half-bridge circuits consisting of a PNP transistor acting as high-side switch  $Q_H$  and NPN transistors acting as low-side switches  $Q_L$  and  $Q_P$ . The low-side switches are used to turn the PNP on and off

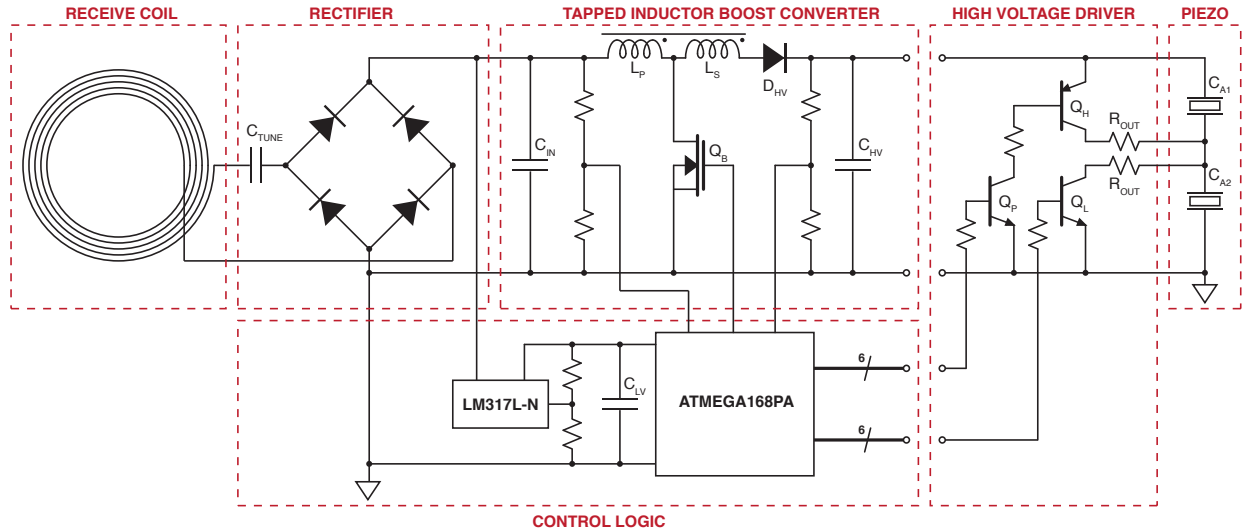


Fig. 9. A schematic of HAMR electronics.

in a simple push-pull configuration. The square-wave output of the half-bridge is filtered by the RC network formed by resistors  $R_{OUT}$  and the actuator capacitances. The control signals to  $Q_L$  and  $Q_P$  are generated, with precise timing to achieve the desired gait frequency and direction, by the Atmel microcontroller. In this work, HAMR’s actuators are driven with quasi-square wave signals (i.e. square waves with an RC delay). However, the same circuit architecture can be used to generate arbitrary drive signal waveforms via pulse width and pulse frequency modulation techniques, as described previously in [22].

### C. PCB Fabrication

The circuits of Fig. 9 are instantiated physically on two PCBs, an upper “control” PCB housing the rectifier, the power conversion circuits, and the Atmel microcontroller, and a lower “drive” PCB containing the high-voltage drive circuits and serving as an electrical and mechanical connection for the piezoelectric actuators. The upper PCB is 5-mil FR4 with a 1/2 oz. copper layer on one side, while the lower PCB is similar but has copper on both sides (the back side of the board is used exclusively for a ground connection). To minimize weight, the smallest available packages are used for the circuit components. Due to the small size of the components and the fact that the manufacturers’ clearance guidelines must occasionally be violated to minimize the board footprint, custom lithography and solder reflow processes are required to produce the boards. All of the circuit components are off-the-shelf with the exception of the receive coil and the tapped inductor. The former is hand-wound using a custom laser-cut jig, while the latter uses a ferrite bobbin core salvaged from the Coilcraft LPS5030 series of power inductors and a custom winding tool to form the primary and secondary windings  $L_P$  and  $L_S$ .

PCB lithography and board outline machining are performed using the same DPSS laser used to produce the mechanical components. Two additional laser-machined com-

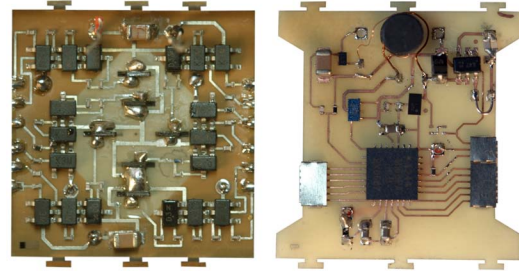


Fig. 10. Completed drive board (right) and control board (left).

ponents assist with PCB population: a solder mask made from 1 mil Kapton tape facilitates solder paste application, and an alignment jig made from FR4 aids in component placement and alignment during the reflow process. The populated board is preheated on a hot plate at 180°C for 10 minutes and reflowed in a Puhui T-962A infrared reflow oven according to component and solder specifications.

After reflow, the alignment jig is removed, and a final DPSS laser cut removes sacrificial alignment features from the boards. In the current version of the process, vias are soldered manually. Fig. 10 shows the completed drive and control boards.

### D. Integration

The PCBs serve as a structural component of HAMR. After the pop-up mechanical structure of Fig. 8 is deployed, tabs on the sides of the PCBs are locked into slots in the sides of the exoskeleton (outer sub-laminates in Fig. 8). The drive board serves as a mechanical ground for the piezoelectric actuators, which are oriented parallel to the sub-laminates and secured in slots in the board. Contact pads on the actuators are soldered to pads on the drive board. An auxiliary FR4 layer with similar slots secures the actuators on the bottom side of the robot. The control board is locked into the exoskeleton above the drive board and provides additional exoskeletal reinforcement.

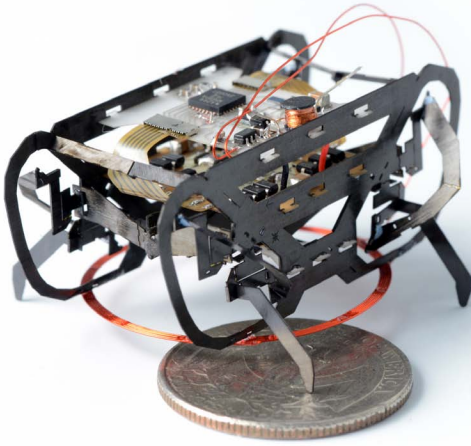


Fig. 11. A fully assembled HAMR with onboard electronics and wireless power components.

The control and drive board are connected with flex cables made from copper-laminated Kapton via the same lithography process used to manufacture the boards. The cables are secured permanently to the drive board and attached to the control board using custom, laser-machined stainless steel connectors weighing less than 5mg each. The receive coil is soldered manually to the control board and can be positioned in various orientations on the exoskeleton using a temporary or permanent mounting adhesive.

#### IV. RESULTS

A fully assembled HAMR with onboard electronics and wireless power components is shown in Fig. 11. The robot weighs 2.1g, including a 275mg control board, 400mg drive board, and 180mg receive coil. As an initial demonstration of wireless power transmission, HAMR is programmed to commence open-loop locomotion at various gait frequencies whenever sufficient power is available to maintain the high-voltage rail to the actuators (configured at a conservative 195V in the current prototype of the control board). Fig. 12 shows HAMR achieving wirelessly powered locomotion in both the single high-efficiency transmit coil scenario and the multiple relay coil scenario described in Section II. In both cases, the transmit coils are driven by a KAA2030M20 power amplifier from AR Modular. Due to the fact that HAMR is running open-loop, it is unable to compensate for deviations from straight-line locomotion. As a result, some degree of sideways drift can be observed in Fig. 12.

The combined weight of the onboard electronics and transmit coil brings HAMR close to the limits of its payload capacity. As a result, the prototype used in this work is not able to achieve the highest speeds demonstrated by tethered versions of HAMR [23] and is limited to about 0.5 body lengths per second. However, the ability to achieve locomotion in two wireless power transmission scenarios supports



Fig. 12. Composite image of several video frames showing HAMR crawling on a clear acrylic sheet 5cm above the blue transmit coil (top), and an image of HAMR crawling on a relay coil, over 40cm from the center of the actively driven coil on the right (bottom). Both cases are at 20Hz gait frequency.

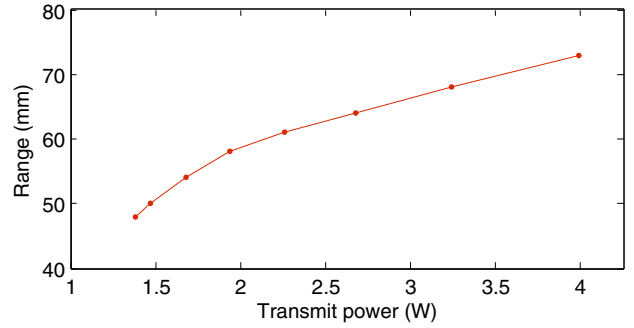


Fig. 13. Wireless power transmission range as a function of transmit power (measured at 1Hz gait frequency).

the feasibility of wireless power for microrobotic applications. Locomotion performance can be improved by applying previously developed weight reduction techniques [24] to onboard electronic components and by reducing the number of manual assembly steps, which can compromise mechanical performance and add unnecessary weight (e.g. solder).

Fig. 13 shows the wireless power transmission range as a function of transmit power for the single transmit coil scenario (blue coil). Higher range is attainable at the cost of decreasing power transmission efficiency (for example, the amplifier used in this experiment can deliver 100W). Increasing range while maintaining efficiency necessitates a larger receive coil, as noted in Section II.

The range measurements of Fig. 13 are performed with the transmit and receive coils oriented parallel to each other and axially aligned. The effects of changing the relative angle of the coils or introducing a horizontal offset distance have not been fully characterized; however, preliminary results indicate that the coil arrangement in the single-coil scenario can tolerate over 4cm offset distance and up to 45° of misalignment.

## V. SUMMARY AND FUTURE WORK

This paper presents the first demonstration of RF wireless power transmission in an insect-scale quadrupedal robot. The work focuses on designing a wireless power transmission system capable of providing sufficient power to the HAMR microrobotic platform, implementing modular power and control electronics with minimal weight and footprint, and system integration. The result is a 2.1g robot that can operate autonomously in two wireless power transmission scenarios.

Future work will focus on improving locomotion performance through weight reduction techniques and demonstrating more complex behaviors. These improvements are expected to pave the way for implementing wireless power in microrobotic platforms with smaller payload capacities, such as RoboBees [25]. Other avenues of exploration include orthogonal transmit coil arrangements (or, alternatively, orthogonally oriented receive coils), which can enable wireless operation in scenarios where the movement of the microrobot will cause substantial changes in the relative angle between the transmit and receive coils. Scenarios where wireless power transmission complements an onboard battery, rather than replacing it, may be investigated. Here, the microrobot could seamlessly transition from full wireless power to battery power with continuous wireless recharging, to full battery power as the robot moves further from the nearest available transmitter. Finally, far-field RF techniques could potentially enable much longer range than the near-field approach demonstrated here, at the cost of efficiency.

## ACKNOWLEDGEMENTS

The authors gratefully acknowledge support from the Wyss Institute for Biologically Inspired Engineering, the Micro Autonomous Systems and Technology (MAST) Collaborative Technology Alliance, and the NSF Engineering Research Center for Sensorimotor Neural Engineering (CSNE), NSF Award EEC-1028725.

## REFERENCES

- [1] M. Karpelson, J. Whitney, G.-Y. Wei, and R. Wood, "Energetics of flapping-wing robotic insects: towards autonomous hovering flight," in *IEEE/RSJ Int. Conf. on Intelligent Robots and Systems*, Oct. 2010, pp. 1630–1637.
- [2] R. J. Full, D. A. Zuccarello, and A. Tullis, "Effect of variation in form on the cost of terrestrial locomotion," *Journal of Experimental Biology*, vol. 150, no. 1, pp. 233–246, 1990.
- [3] A. T. Baisch, C. Heimlich, M. Karpelson, and R. J. Wood, "HAMR<sup>3</sup>: An autonomous 1.7g ambulatory robot," in *IEEE/RSJ Int. Conf. on Intelligent Robots and Systems*, Sept. 2011, pp. 5073–5079.
- [4] O. Ozcan, A. Baisch, and R. J. Wood, "Design and feedback control of a biologically-inspired miniature quadruped," in *IEEE/RSJ Int. Conf. on Intelligent Robots and Systems*, 2013.
- [5] A. Baisch and R. J. Wood, "Pop-up assembly of a quadrupedal ambulatory microrobot," in *IEEE/RSJ Int. Conf. on Intelligent Robots and Systems*, 2013.
- [6] R. J. Wood, E. Steltz, and R. S. Fearing, "Optimal energy density piezoelectric bending actuators," *Sensors & Actuators: A. Physical*, vol. 119, no. 2, pp. 476–488, 2005.
- [7] T. Deyle and M. Reynolds, "Surface based wireless power transmission and bidirectional communication for autonomous robot swarms," in *IEEE Int. Conf. on Robotics and Automation*, 2008, pp. 1036–1041.
- [8] J. Gao, "Inductive power transmission for untethered micro-robots," in *31st Annual Conf. of the IEEE Industrial Electronics Society*, 2005.
- [9] R. Carta and R. Puers, "Wireless power and data transmission for robotic capsule endoscopes," in *IEEE Symp. on Communications and Vehicular Technology in the Benelux (SCVT)*, 2011, pp. 1–6.
- [10] A. Sample, D. Yeager, P. Powledge, A. Mamishev, and J. Smith, "Design of an RFID-based battery-free programmable sensing platform," *IEEE Transactions on Instrumentation and Measurement*, vol. 57, no. 11, pp. 2608–2615, 2008.
- [11] H. Zeine, "Wireless power transmission system," Oct. 2013, US Patent 8,558,661.
- [12] B. Cannon, J. Hoburg, D. Stancil, and S. Goldstein, "Magnetic resonant coupling as a potential means for wireless power transfer to multiple small receivers," *IEEE Transactions on Power Electronics*, vol. 24, no. 7, pp. 1819–1825, 2009.
- [13] A. Sample, D. Meyer, and J. Smith, "Analysis, experimental results, and range adaptation of magnetically coupled resonators for wireless power transfer," *IEEE Transactions on Industrial Electronics*, vol. 58, no. 2, pp. 544–554, 2011.
- [14] A. Sample, B. Waters, S. Wisdom, and J. Smith, "Enabling seamless wireless power delivery in dynamic environments," *Proceedings of the IEEE*, vol. 101, no. 6, pp. 1343–1358, 2013.
- [15] J. Casanova, Z. N. Low, and J. Lin, "A loosely coupled planar wireless power system for multiple receivers," *IEEE Transactions on Industrial Electronics*, vol. 56, no. 8, pp. 3060–3068, Aug. 2009.
- [16] D. Ahn and S. Hong, "A study on magnetic field repeater in wireless power transfer," *IEEE Transactions on Industrial Electronics*, vol. 60, no. 1, pp. 360–371, Jan. 2013.
- [17] K. Hoffman and R. Wood, "Passive undulatory gaits enhance walking in a myriapod millirobot," in *IEEE/RSJ Int. Conf. on Intelligent Robots and Systems*, Sept. 2011, pp. 1479–1486.
- [18] P. Sreetharan, J. Whitney, M. Strauss, and R. Wood, "Monolithic fabrication of millimeter-scale machines," *Journal of Micromechanics and Microengineering*, vol. 22, no. 055027, 2012.
- [19] A. Baisch, P. Sreetharan, and R. Wood, "Biologically-inspired locomotion of a 2g hexapod robot," in *IEEE/RSJ Int. Conf. on Intelligent Robots and Systems*, Oct. 2010, pp. 5360–5365.
- [20] N. Vazquez, L. Estrada, C. Hernandez, and E. Rodriguez, "The tapped-inductor boost converter," in *IEEE Int. Symposium on Industrial Electronics*, 2007, pp. 538–543.
- [21] "Small, high-voltage boost converters," Maxim Semiconductor Application Note 1109, 2002.
- [22] M. Karpelson, G.-Y. Wei, and R. J. Wood, "Milligram-scale high-voltage power electronics for piezoelectric microrobots," in *IEEE Int. Conf. on Robotics and Automation*, 2009, pp. 883–890.
- [23] A. T. Baisch, O. Ozcan, B. Goldberg, D. Ithier, and R. J. Wood, "High speed locomotion for a quadrupedal microrobot," *to appear: Int. J. of Robotics Research*, 2014.
- [24] M. Karpelson, J. P. Whitney, G.-Y. Wei, and R. J. Wood, "Design and fabrication of ultralight high-voltage power circuits for flapping-wing robotic insects," in *Applied Power Electronics Conf.*, 2011.
- [25] K. Ma, P. Chirarattanon, S. Fuller, and R. J. Wood, "Controlled flight of a biologically inspired, insect-scale robot," *Science*, vol. 340, pp. 603–607, 2013.